PANAMGEO CHILE 2024
17th PAN-AMERICAN CONFERENCE ON SOIL MECHANICS AND GEOTECHNICAL ENGINEERING | 2nd LATIN-AMERICAN REGIONAL CONFERENCE OF IAEG
LA SERENA • CHILE / NOVEMBER 12 - 16, 2024

Proceedings of the 17th Pan-American Conference on Soil Mechanics and Geotechnical Engineering (XVII PCSMGE), and 2nd Latin-American Regional Conference of the International Association for Engineering Geology and the Environment (IAEG), La Serena Chile, 2024.

Evaluation and prediction of regional subsidence in Mexico City

Evaluación y predicción del hundimiento regional en la Ciudad de México

Haydee Román, Marcos Delgado, Moisés Juárez & Gabriel Auvinet
Engineering Institute, Geoinformatics Laboratory, UNAM, Mexico City, Mexico, HRomanR@iingen.unam.mx.

ABSTRACT: In this paper, the evaluation of the regional subsidence of Mexico City based on leveling data is presented. The analysis consists of a detailed study of the spatial distribution of the ground elevations, using annual measurements on approximately 1127 benchmarks distributed in the lacustrine zone of Mexico Valley, from the year 1983 to 2017. The spatial distribution of subsidence was assessed using the univariate (kriging) geostatistical methodology. Subsequently, the punctual prediction of the subsidence rate in each benchmark was calculated using the linear regression technique. The subsidence rates were used to obtain predictions (extrapolations) for the years 2025, 2030, 2040 and 2050 respectively. As a result, the present and future spatial distribution of the regional subsidence in Mexico City and contour maps of the terrain elevation are presented.

KEYWORDS: regional subsidence, subsidence rate, terrain elevation, geostatistics, kriging.

1 INTRODUCTION

Land subsidence is a geological phenomenon which is caused by the consolidation and compression of subsurface unconsolidated materials, leading to a decrease in ground elevation (Zamanirad *et al*., 2019). Intensive exploitation of aquifers has been identified as the main cause of land subsidence in many cities around the world (Aviles and Pérez, 2010). Currently, land subsidence has been observed in more than 200 countries and regions, such as Mojave Desert of California, USA (Galloway *et al*., 1998), Mexico city (Auvinet *et al*., 2017; Auvinet *et al*., 2019), central Indonesia (Marfai and King, 2007) and the Beijing-Tianjin-Hebei region of China (Gong *et al*., 2018).

It is known that the Valley of Mexico is a closed basin, the floor of which was occupied by a series of interconnected lakes prior to the construction of an artificial drainage system in the late 1780s (Bribiesca, 1960). Subsidence of the city began to be noticed in the late XIXth and early XXth centuries. It was first described in 1925 by Roberto Gayol responsible for the construction of the main sewage channel of Mexico city (Figueroa, 1984).

The regional subsidence of the Valley of Mexico phenomenon occurs particularly in the so-called Lake and Transition Zones and is associated with the pumping of underground water from the deep aquifers. The subsidence contributes to the evolution of the properties of the subsoil (Auvinet, 2019). The effects of future regional subsidence on the seismic response have been evaluated and shown to be very significant (Ovando *et al*., 2007). It has been recognized that, in the future, it will be necessary to modify the building code seismic requirements to consider this evolution.

On the other hand, the subsidence generates damages to drainage and transport systems as well as to other services of the city and severe foundation behavior problems (Auvinet *et al*., 2017). In addition, the subsidence is associated with the appearance of cracks in the ground in abrupt transition zones, especially in the contact between soft and rigid materials around volcanic ranges. Cracks and differential settlements with steps that can exceed 50 cm have developed progressively and created a critical geotechnical environment. These fissures affect street pavement, public services and constructions (Auvinet *et al*., 2019).

In this paper, the geostatistical methodology used to evaluate the evolution of the regional subsidence in Mexico City is presented. Using available measurements of the elevation of benchmarks distributed in the Mexico Valley, contour maps representing the evolution of the settlement and subsidence rate have been established for different years. Additionally, predictions for the future years considering the trend of the subsidence rate are presented.

2. SUBSIDENCE RATE

The hypothesis of constant subsidence rate (*vs*) can be objected since, in the case of a consolidation process, it is expected that this parameter will tend to decrease over time. However, this hypothesis is acceptable for time intervals that can span several decades, as long as there is no significant change in pumping policy. The hypothesis has greater validity in areas where the thickness of clay in the consolidation process is important. It is known that these areas correspond precisely to those with the highest rate of sinking (Pérez, 2009). The subsidence rate (*vs*) during the observation period was first estimated for each benchmark. The parameter *vs* is the relation between the elevations and the number of years, the expression for *vs* is:

$$vs_{1-2} = 100\frac{\Delta H_{1-2}}{t_2 - t_1} \quad (1)$$

where

$$\Delta H_{1-2} = \left(Z_1\right) - \left(Z_2\right) \quad (2)$$

$\Delta H_{1\text{-}2}$ is the regional subsidence during the time interval (msl), Z_1 and Z_2 are the benchmarks elevation measurements (msl); t_1 and t_2 are the time instants in years.

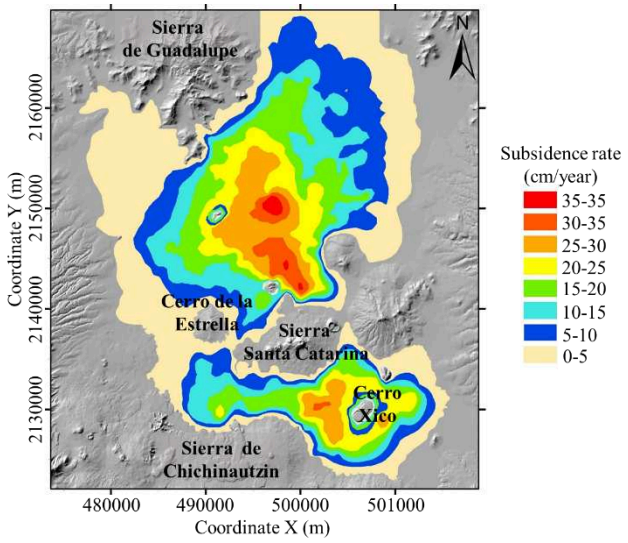

Figure 1. Contour map of the estimated subsidence rate (Juárez *et al.*, 2021).

2.1. *Elevation prediction*

To obtain elevations to years 2020, 2030, 2040, and 2050, the subsidence rate was multiplied by number of years in the period and subtracted from the last measured elevation (2017).

$$Z^*(X) = Z(X) - [vs \cdot t] \quad (3)$$

where: Z^* is the estimated elevation (msl), Z is the measured elevation (msl), vs is subsidence rate (cm/year), t is time of the prediction (year). Through equation 3, the new elevations for different years were determined.

3. GEOSTATISTICS

3.1. *Random fields*

Let us consider a geotechnical variable $V(X)$, either of physical (i.e. water content), mechanical (i.e. shear strength) or geometrical (i.e. depth, elevation or thickness of some stratum) nature defined at points X of a given domain R^p (p = 1, 2, or 3). In each point of the domain, this variable can be considered as random due to the range of possible values that it can take. The set of these random variables constitutes a random field (Vanmarcke, 1983; Auvinet, 2002).

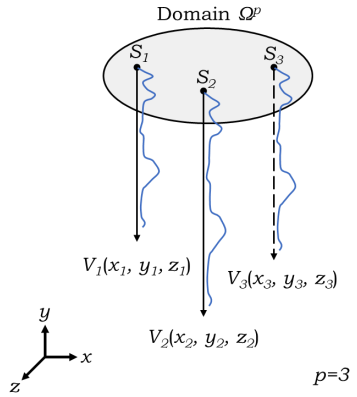

Figure 2 Schematic representation of the random field (Auvinet, 2002).

3.2. *Kriging*

The kriging estimation technique, also known as BLUE (best linear unbiased estimator, for its acronym in English) consists in using the estimator defined by next equation:

$$V^*(X) = \sum_{i=1}^{n} \lambda_i V(X_i) + \left[1 - \sum_{i=1}^{n} \lambda_i\right] \mu_v \quad (4)$$

where λ_i are the influence weights and μ_v is the expected value of the random field. One of the variants of the kriging estimation is the ordinary kriging (*OK*), where imposing the condition $\Sigma\lambda_i$=1 in the equation (4), makes it not unnecessary to know the mean value μ_v of the random field (Deutsch and Journel, 1992). The estimation equation of ordinary kriging is then defined as:

$$V^*(X) = \sum_{i=1}^{n} \lambda_i V(X_i) \quad (5)$$

The value of the minimized error variance associated to the estimation (σ^2_{OK}), is obtained with the following expression:

$$\sigma^2_{OK}(X) = Var[V(X)] + \mu_v - \sum_{i=1}^{n} \lambda_i C(X_i) \quad (6)$$

4. METHODOLOGY

In general, the geostatistical methodology is integrated by four stages: i) exploratory analysis, ii) trend analysis ii) structural analysis and iv) prediction (Delgado *et al.*, 2019). To analyze and interpret the subsidence and the spatial configuration of the ground elevation, the theoretical foundation of the geostatistical analysis (univariable) is adapted, and a series of stages are defined as indicated in Figure 3.

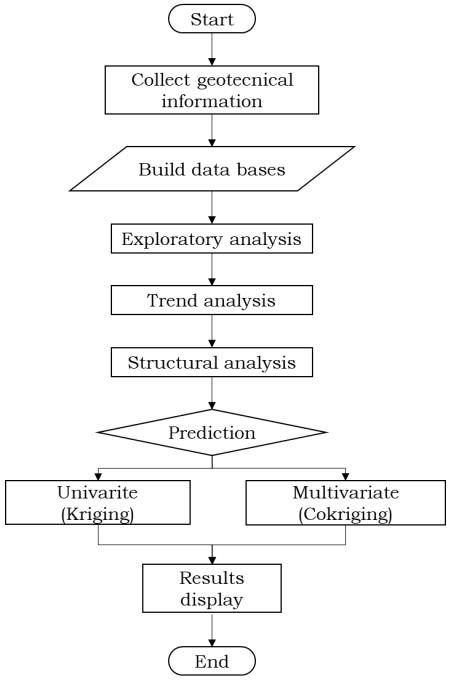

Figure 3. Flowchart of the geostatistical methodology (Delgado *et al.*, 2019)

5 APPLICATION

5.1 *Study area*

Geologically, the so-called Valley of Mexico is a closed basin located in the highest part and southern end of the Mexican plateau. It is located between parallels 19°00' and 20°12' north and meridians 98°10' and 99°33' west. It is bounded on the north by the mountains of Tepotzotlan, Tezontlalpan and Pachuca, east by the plains of Apan and the Sierra Nevada, south by the mountains of Chichinautzin and Ajusco and west by Sierras de Las Cruces, Monte Alto and Monte Bajo. Its surface is around 9600 km^2, of which only 30% is flat (Auvinet, 2019).

Geotechnically, the urban area of Mexico Valley is divided in three main zones (Marsal, 1975): Foothills (Zone I), Transition (Zone II) and Lake (Zone III). In the foothills, very compact but heterogeneous volcanic soils and lava are found. These materials contrast with the highly compressible soft soils of the Lake Zone. Generally, in between, a Transition Zone is found where clayey layers of lacustrine origin alternate with sandy alluvial deposits (Auvinet, 2019).

For monitoring subsidence in the city, a network of around 1127 benchmarks distributed throughout the transition and soft zones has been installed, as seen in Figure 4. The information of the network of benchmarks in the Mexico City was provided by different entities: Mexico City Water System (SACMEX), Organismo de Cuenca del Valle de México (OCAVAM), Water Commission of the State of Mexico (CAEM) and Mexico City Airport Group (GACM).

5.2 *Definition of the random fields*

The ground elevation (Z) and subsidence rate (sv) are considered to be random fields $V(X)$ and $S(X)$ respectively, defined within R^p, with p=2 (2D case). The Z and sv values set measured and calculated within the domain R^2, constitute samples from that random fields. The distribution of level benchmarks in the study area is shown in Figure 4.

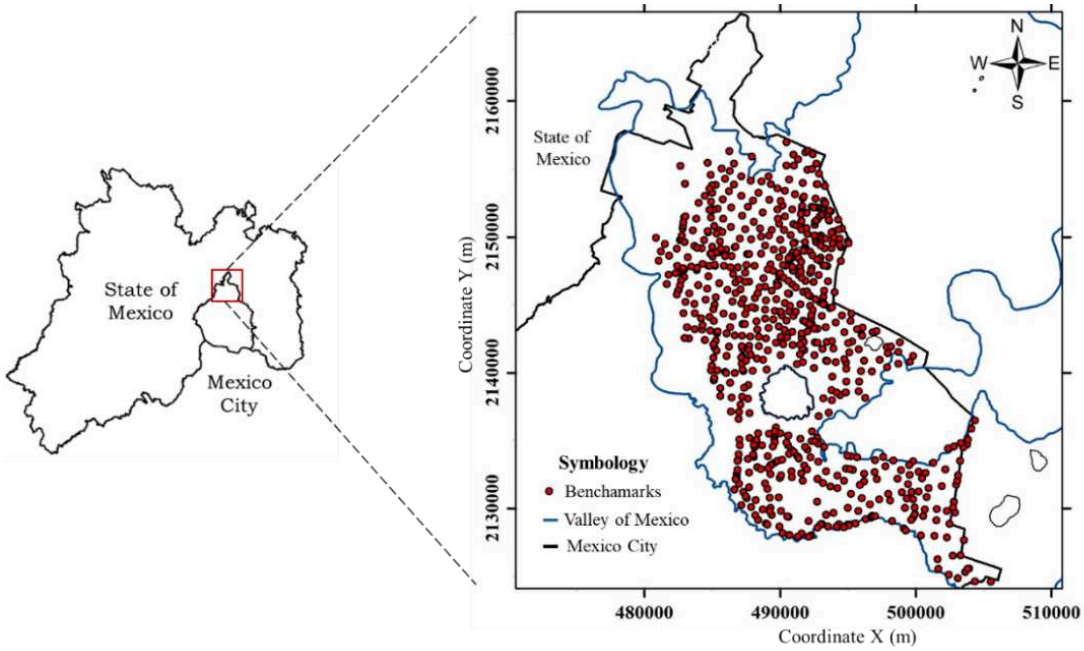

Figure 4. Location of the study area and distribution of benchmarks.

5.3 *Exploratory analysis*

In this stage of the geostatistical analysis, the aim is to identify the atypical values (*outliers*) that affect the subsequent stages of the methodology (Figure 3) and obtain the main statistical parameters of the properties or attributes.

Based on the above, a detailed review of the elevation measurements for each of the benchmarks was carried out, with the objective of evaluating the consistency in the measurements in the time domain. The review included a linear regression analysis adopting the following equation:

$$y = ax + b \tag{7}$$

where y is the elevations (msl), x is the time (years), a and b are the linear coefficients

In addition, graphs were made of the time versus elevation measurements as shown in Figure 5. In each graph the coefficient of determination R^2 is indicated. A R^2 value equal to 1 means a perfect linear fit, a value of zero indicates the non-representativeness of the linear model. In this work, a minimum R^2 value of 0.95 was established as a limit to use the elevation measurements of the benchmarks in the next stages of the analysis.

In addition to the previous data filter, it was also decided to discard the measurements of the benchmarks with the following conditions, i) installed in the Foothills geotechnical zone (Figure 5c), ii) with relocations that do not allow detecting acceptable subsidence trends, iii) with measurements that show apparent protruding (Figure 5d) and iv) with intermittent or recently installed measurements.

In accordance with the previous points and after a careful cleaning of the data, the elevation prediction analysis and the geostatistical analysis were carried out with 1127 of the 2621 benchmarks installed in the Valley of Mexico.

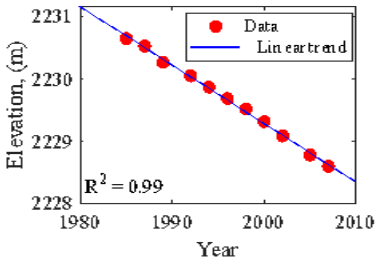

a) Benchmark (BN1) with linear trend.

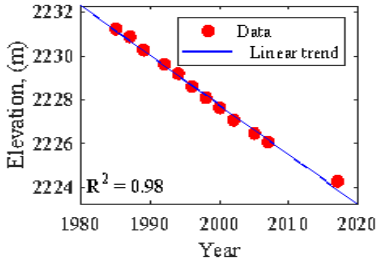

b) Benchmark (BN2) with linear trend.

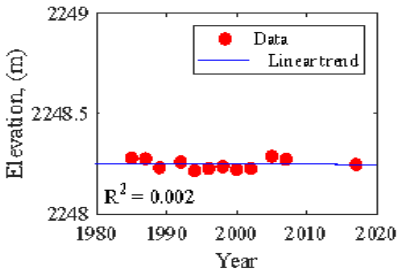

c) Benchmark (BN3) installed in the foothills zone

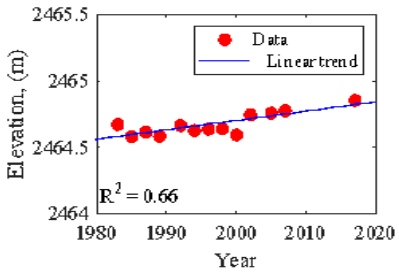

d) Benchmark (BN4) with apparent protruding.

Figure 5. Trend plot of the yearly elevation measurement for different year o benchmarks.

Considering the 1127 elevation measurements of the experimental data and assuming ergodicity of the random fields, the main geostatistical parameters of these fields were obtained and synthetized in Table 1.

Table 1. Statistical parameters of the elevation measurements per year.

Parameter, (m)	Year				
	2020	2025	2030	2040	2050
Mean	2230.5	2228.5	2227.9	2226.5	2225.1
Median	2229.6	2228.4	2227.9	2226.6	2225.4
Mode	2229.0	2229.0	2227.5	2229.0	2227.5
Standard deviation	6.7	5.1	5.6	6.5	7.4
Minimum value	2219.5	2218.1	2216.7	2213.8	2210.4
Maximum value	2247.2	2239.9	2240.0	2239.9	2239.9

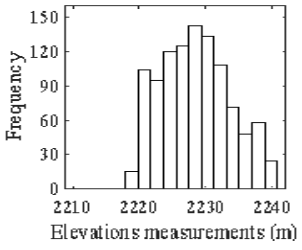

a) Histogram of year 2025

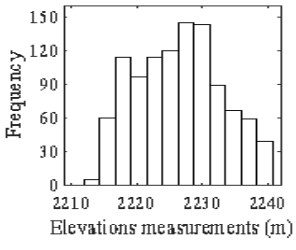

b) Histogram of year 2030

Figure 6. Histograms of elevations measurements for different years.

5.4 *Trend analysis*

In this step of the geostatistical methodology, the trend of the random fields is assumed to be approximately represented by a surface with linear equation $V(X)=ax+by+c$ where "a, b, and c" are linear regression coefficients (Table 3).

Table 2. Regression linear coefficients of the elevations per year.

Year	*a*	*b*	*c*
2020	-3.81E-04	-3.27E-04	3119.04
2025	-4.10E-04	-3.47E-04	3176.08
2030	-2.95E-04	-3.10E-04	3037.18
2040	-3.49E-04	-3.28E-04	3100.89
2050	-3.98E-04	-3.49E-04	3169.37

The linear coefficients of Table 2 allow removing the trend from the Z data in order to work with simpler stationary residual fields In Figure 5 the trend of the random field is represented by a surface, where it can be seen that, to the west, the elevation is higher and that it decreases towards the center of Mexico City. The trend is returned in the stage of the estimation.

5.5 *Structural analysis*

Considering the data of the residual fields, the directional correlograms in the azimuth directions 0°, 45°, 90° and 135° were calculated; the correlation distances are presented in Table 4.

Table 3. Directional correlations distances of the elevation per year.

Azimuth. directions	Correlation distances, δ (m)				
	2020	2025	2030	2040	2050
0°	60000	75000	80000	7800	7500
45°	40000	25000	12000	7800	7500
90°	75000	75000	75000	7800	7500
135°	35000	30000	30000	7800	7500

With the correlation distances and adopting a simple exponential correlation model, the correlograms in the preferential directions (0º, 45º, 90º and 135º) of the residual fields were determined. Figure 7 shows the directional correlograms of the structural analysis for the elevation distribution analysis for year 2040.

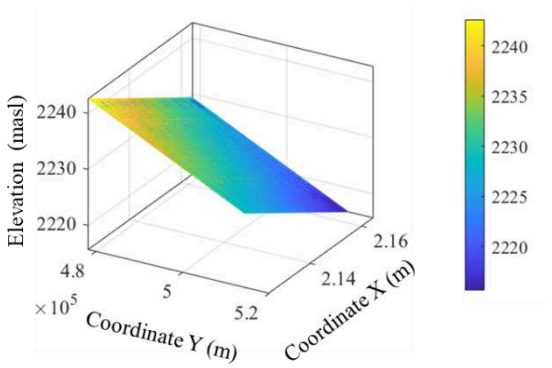

a) Trend surface of the elevations for year 2025.

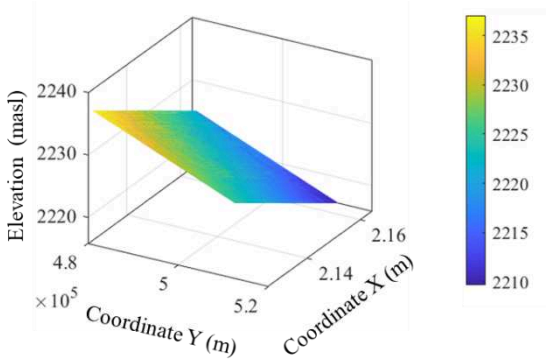

b) Trend surface of the elevations for year 2030.

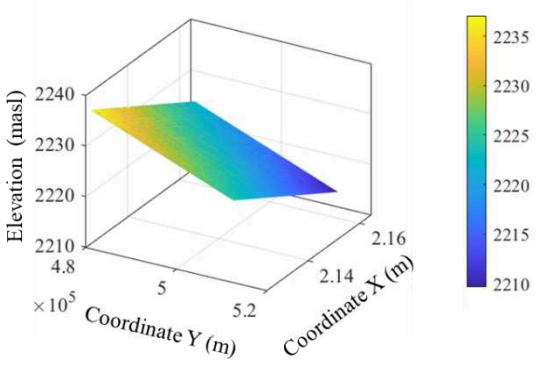

c) Trend surface of the elevations for year 2040.

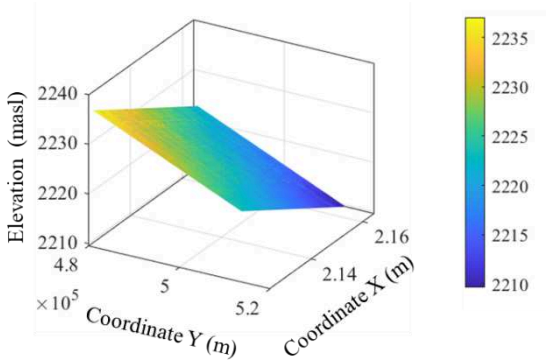

d) Trend surface of the elevations for year 2050.

Figure 7. Trend surface of the random fields of elevation.

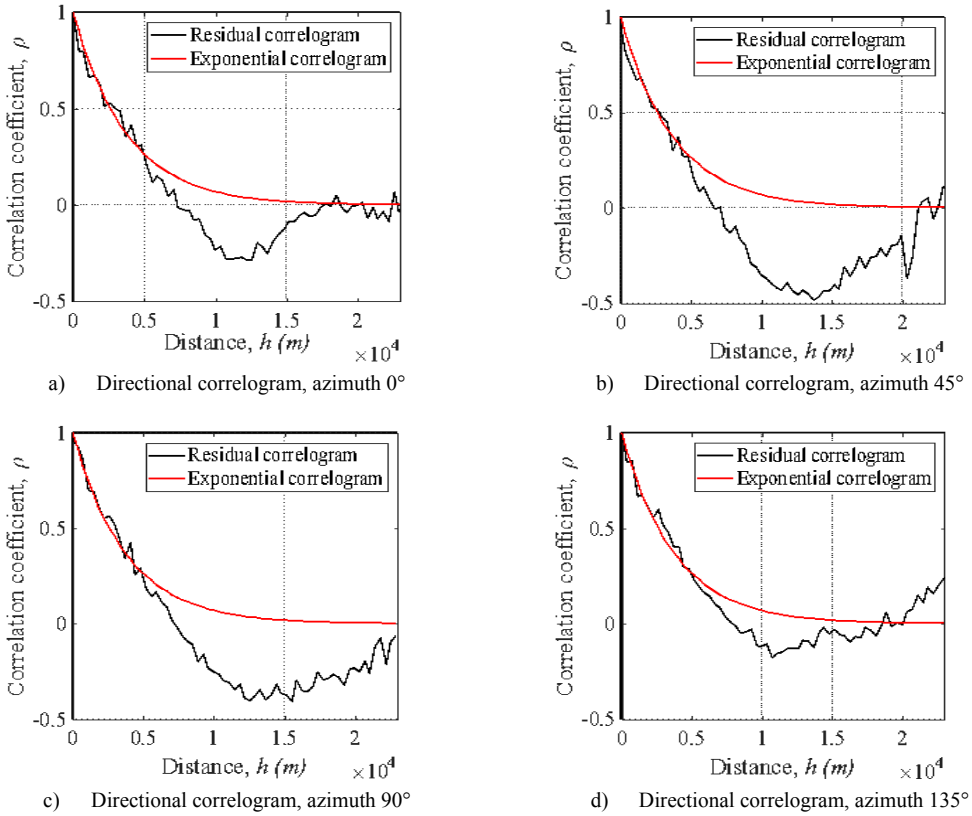

a) Directional correlogram, azimuth 0°

b) Directional correlogram, azimuth 45°

c) Directional correlogram, azimuth 90°

d) Directional correlogram, azimuth 135°

Figure 8. Directional correlograms of the elevations for the year 2040.

.

5.6 *Prediction*

The estimation of the evolution of the subsidence phenomena in terms of the terrain elevations (random field R^2) was carried out using the Ordinary Kriging technique for the years 2020, 2030, 2040, and 2050, considering the residual field data and the corresponding correlation distances previously calculated. To obtain the final estimate, the trend was reincorporated into the estimate obtained, using the corresponding linear regression coefficients. The estimation mesh used completely covers the study surface. The estimation mesh considered, in this case, an equidistant calculation step of 500m in both X and Y directions.

The estimation domain is delimited by the perimeters of the Guadalupe, Santa Catarina, Las Cruces and Chichinautzin mountain ranges with elevation 2240 msl, as well as the Estrella, Xico, Tlapacoyán, Peñón del Baño and Peñón del Marqués hills, within the Valley of Mexico. From this level, it is noticeable how the elevations decrease as the point of interest moves away from the hills; It can also be seen that the lowest levels are found in the areas where the subsidence rate is highest.

To simplify the interpretation of the tabular values of different configurations of the terrain elevation (regional subsidence) obtained in the estimation stage, we resort to graphics techniques that allow the construction of contours that facilitate the visualization of the evolution of the regional subsidence in Mexico City. In Figures 9, the elevation maps are presented taking as reference the 2017 measurements, as well as the estimated elevations corresponding to different years: 2020, 2025, 2030, 2040 and 2050.

In Figure 9, contour maps are presented with the spatial distribution of the elevations with the same color scale to appreciate in detail the evolution of the subsidence phenomenon for the different years of analysis. For the year 2017 (Figure 9a) the lowest elevations are observed with a magnitude of the order of 2223 msl, south of Cerro del Peñón, Mexico City International Airport (AICM) and at the center of the former Texcoco lake. In map of Figure 9b, it can be seen that the area with the lowest elevation values extends and that there is a decrease in elevation of one meter. In Figure 9c, the contour map for the year 2025, a decrease in elevation is observed, where the minimum values are on the order of 2021 msl. In Figure 9d, the area affected by the subsidence phenomenon extends and descends another meter, reaching a minimum elevation of 2020 msl. Furthermore, in the southern area of the Valley, in Lake Xochimilco, the problem is more evident, in this area the subsidence rate ranges from 25 to 35 cm/year. Figure 9e shows a decrease in ground elevation of four meters in the areas with the largest settlements.

Finally, in Figure 9e, for the year 2050, it can be seen that the areas most affected by the subsidence phenomenon are: the Peñon del Marqués with an elevation of 2212 msl, the Mexico City International Airport with an elevation of 2214 msl and, to the south in Xochimilco, the elevation is 2218 msl.

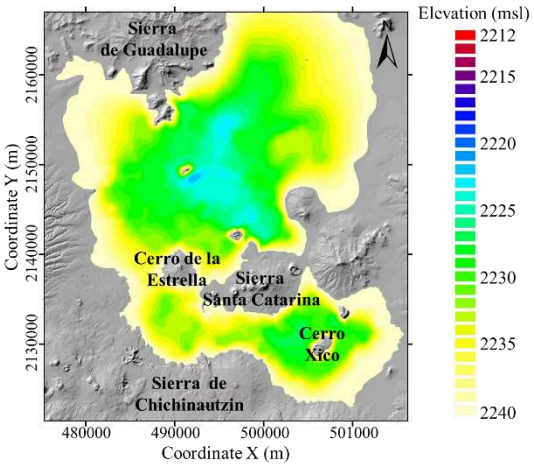

a) Contour map of elevation with the subsidence estimated for the year 2017.

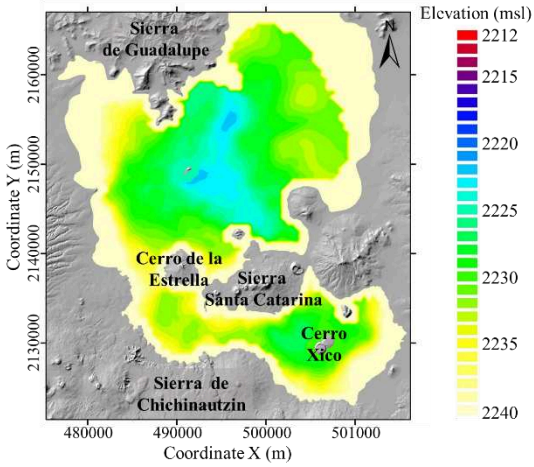

b) Contour map of elevation with the subsidence estimated for the year 2020.

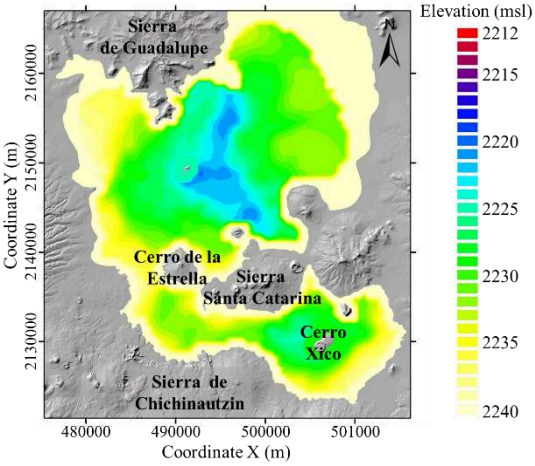

c) Contour map of elevation with the subsidence estimated for year 2025

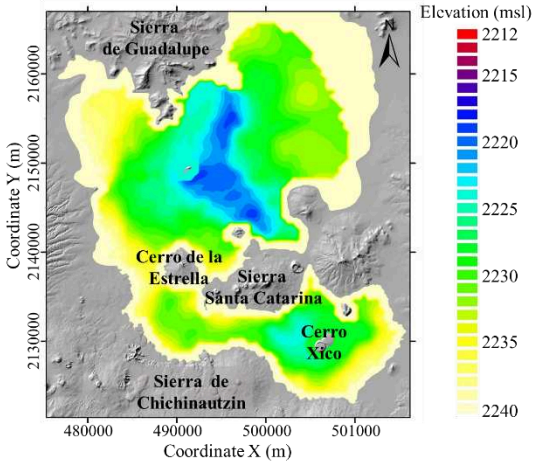

d) Contour map of elevation with the subsidence estimated for year 2030.

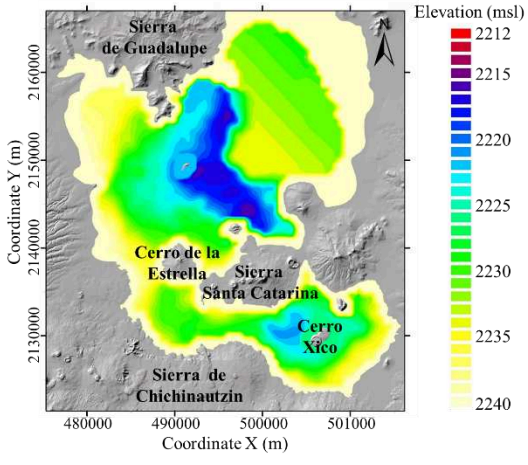

e) Contour map of elevation with the subsidence estimated for year 2040.

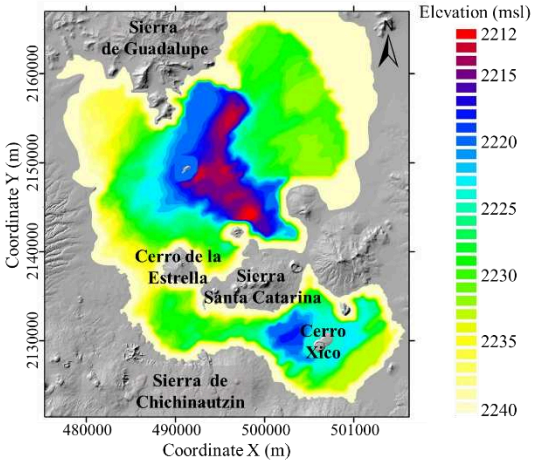

f) Contour map of elevation with the subsidence estimated for year 2050.

Figure 9. Contour maps of elevation considering the regional subsidence estimated for years 2017, 2020, 2025, 2030, 2040 and 2050.

6. CONCLUSIONS

The evolution of regional subsidence in Mexico City was evaluated. In view of the complexity of the phenomenon, the geostatistical methodology was applied as a useful tool for the interpretation of information obtained from benchmarks. This technique can be used for the characterization of areas of large extensions, considering the existing correlation between the measurements.

In the contour maps obtained by estimations of the spatial distribution of the elevations for different years, the evolution of the subsidence mechanism for different future dates can be appreciated. It should be expected that the unevenness between different parts of the city will be significantly accentuated, which can favor flooding, damage to roads, buildings and works. of infrastructure and the appearance of cracks.

In the areas with higher settlement where the velocity gradients have notable increases for the period 2017 to 2050, the foreseeable additional settlement is of the order of 11 meters.

The methodology proposed and used in this work for the predictions constitutes a simple and reliable alternative to calculate, analyze and visualize the future projection of elevation maps, but it must be kept in mind that they are based on the hypothesis that the water pumping policy will not significantly change in the coming decades.

7. REFERENCES

Auvinet, G. 2002. Uncertainty in Geotechnical Engineering, Sixteenth Nabor Carrillo Lecture, Sociedad Mexicana de Mecánica de Suelos.

Auvinet, G., Méndez, E. and Juárez, M. 2017. El subsuelo de la Ciudad de México. Instituto de Ingeniería, UNAM. ISBN Vol. 3 978-607-02-8198-3.

Auvinet, G. 2019. Geotechnical Engineering in Spatially Variable Soft Soils. The case of Mexico City (9th Arthur Casagrande Lecture), Advances in Soil Mechanics and Geotechnical Engineering.

Avilés, J. and Pérez, L. 2010. Regional subsidence of Mexico City and its effects on seismic response. Soil Dynamics and Earthquake Engineering. 981-989

Bribiesca, J. 1960. Historic hydrology of the Valley of Mexico. Ingeniería Hidráulica en México; 1960; XIV (3): 43–62.

Delgado, M., Juárez M. and Auvinet, G. 2019. Multivariable Geostatistical Analysis of the Geotechnical Properties in the Mexico Valley Subsoil. Geotechnical Engineering in the XXI Century: Lessons learned and future challenges.

Deutsch, C. and Journel, A. 1992. GSLIB, Geostatistical Library and user´s guide. Oxford University Press, New York, USA.

Figueroa, G. 1984. Case history no. 9.8, Mexico DF. In: Poland JF, editor. GuideBook to Studies of Land Subsidence due to Ground-Water Withdrawal. Unesco; Chapter 9.

Galloway, L., Hudnut, K., Ingebritsen, S., Phillips, S., Peltzer, G., Rogez, F. and Rosen P. 1998. Detection of aquifer system compaction and land subsidence using interferometric synthetic aperture radar, Antelope Valley, Mojave Desert, California. Water Resources.

Gong, H., Pan, Y., Zheng, L., Li, X., Zhu, L., Zhang, C., and Zhou, C. 2018. Long-term groundwater storage changes and land subsidence development in the North China Plain (1971–2015). Hydrogeology Journal, 26(5), 1417-1427.

Juárez, M, Román, H. and Auvinet, G. 2021. Contribución a la actualización del mapa de hundimiento regional para el valle de México, XXX Reunión Nacional de Ingeniería Geotécnica, SMIG

Juárez, M, Román, H. and Auvinet, G. 2022. Predicción del hundimiento regional en el Valle de México, XXXI Reunión Nacional de Ingeniería Geotécnica, noviembre, Guadalajara, Jalisco.

Krige, D. 1966. Two-dimensional weighted moving average rend surface for ore valuation, Journal South African Inst. Of Mining and Metallurgy, pp. 13-38.

Marfai, M.A., King, L. 2007. Monitoring land subsidence in Semarang, Indonesia. Environ. Geol. 53 (3), 651–659.

Marsal, R. 1975. The lacustrine clays of the valley of Mexico, Contribution of Instituto de Ingeniería, UNAM to the 1975 International clay conference, Publication E16, Instituto de Ingeniería, Universidad Nacional Autónoma de México, México

Ovando, E., Romo, M and Ossa, A. 2007. The sinking of Mexico City: Its effects on soil properties and seismic response. Soil Dynamics and Earthquake Engineering, 27, No. 4, 333-343.

Pérez, D. 2009. Modelado del hundimiento de la zona lacustre del valle de México. Aspectos estratigráficos y piezométricos, Tesis de Maestría, ESIA-Instituto Politécnico Nacional, Ciudad de México, México.

Vanmarcke, E. 1983. Random fields; Analysis and synthesis, MIT Press, Cambridge, Massachusetts, USA.

Zamanirad, M., Sarraf, A., Sedghi, H., Saremi, A., and Rezaee P. 2019. Modeling the influence of groundwater exploitation on land subsidence susceptibility using machine learning algorithms. Nat. Resour. Res. (1), 1–15.